Composite Structures 106 (2013) 681–689

Contents lists available at SciVerse ScienceDirect

Composite Structures

journal homepage: www.elsevier.com/locate/compstruct

In plane stiffness of multifunctional hierarchical honeycombs with negative Poisson's ratio sub-structures ☆

Yongtao Sun [a], Nicola M. Pugno [b,c,*]

[a] Laboratory of Bio-Inspired Nanomechanics Giuseppe Maria Pugno, Department of Structural, Geotechnical and Building Engineering, Politecnico di Torino, 10129 Torino, Italy
[b] Laboratory of Bio-Inspired & Graphene Nanomechanics, Department of Civil, Environmental and Mechanical Engineering, University of Trento, Via Mesiano 77, Trento I-38123, Italy
[c] Center for Materials and Microsystems, Fondazione Bruno Kessler, Via Sommarive 18, I-38123 Povo (Trento), Italy

ARTICLE INFO

Article history:
Available online 23 May 2013

Keywords:
In-plane stiffness
Original regular hexagonal honeycomb (ORHH)
Multifunctional hierarchical honeycomb (MHH)
Negative Poisson's ratio (NPR)
Re-entrant honeycombs
Chiral honeycombs

ABSTRACT

Compared with triangular, square and Kagome honeycombs, hexagonal honeycomb has superior heat dissipation capabilities, but its lower in-plane stiffness hinders its multifunctional applications. Regarding this problem, in this paper we propose a multifunctional hierarchical honeycomb (MHH) with negative Poisson's ratio (NPR) sub-structures. This MHH is constructed by replacing the solid cell walls of the original regular hexagonal honeycomb (ORHH) with two kinds of equal mass NPR honeycombs, the anisotropic re-entrant honeycomb or the isotropic chiral honeycomb. Based on the Euler beam theory, formulas for the Young's moduli of these two kinds of MHH structures are derived. Results show that by appropriately adjusting the geometrical parameters both the re-entrant honeycomb (when the cell-wall thickness-to-length ratio of the ORHH is less than 0.045) and the chiral honeycomb (when the cell-wall thickness-to-length ratio of the ORHH is less than 0.75) can greatly tune the in-plane stiffness of the MHH structure. The presented theory could thus be used in designing new tailorable hierarchical honeycomb structures for multifunctional applications.

1. Introduction

As one kind of typical low density cellular solids, honeycomb structures have been applied in many fields such as aerospace and automotive industries in which they are mainly used as cores of the light-weight sandwich panel structures [1–4]. In addition to the appealing low-density and specific mechanical properties, honeycombs also have other attractive functionalities, e.g., heat transfer, thermal protection, catalysis application, and so on [5–8]. Referring to the heat transfer properties, comparing with triangular, square and Kagome honeycombs, regular hexagonal metal honeycombs provide the highest level of heat dissipation when used as heat sink media [5,6,9]. However, the regular hexagonal honeycombs have much lower in plane stiffness which greatly restricts their multifunctional applications. To improve the in plane stiffness of regular hexagonal honeycombs, the crucial role on stiffness, strength and toughness that hierarchy plays in both natural and bio-inspired materials has already been exploited [10–22]. Introducing the concept of hierarchy and surface effects of nanoscale into honeycombs, Pugno and collaborators studied elastic properties, in-plane buckling and bending collapses of such new materials [23–25]. Chen and Pugno [26] reviewed the hierarchical structures and mechanisms behind their mechanical properties, from animals (nacre, gecko feet, mussel, spider silk, crabs, armadillo and turtle shells) to plants (diatoms and plant stem). Also, Sun and Pugno [27] proposed hierarchical fibers with a negative Poisson's ratio, which provide a new strategy for the design of fiber reinforced hierarchical bio-inspired composites with a superior friction during the pull-out mechanism, and thus a superior toughness.

Taylor et al. [28,29] introduced functionally graded hierarchical honeycombs, and their finite element results suggested that the elastic modulus of the functionally graded hierarchical honeycomb can be up to 2 times that of its equal-mass first-order hexagonal honeycomb if the structure is designed properly. Different from Taylor's work, Ajdari et al. [30] developed a new hierarchical honeycomb structure by replacing every three-edge joint of a regular hexagonal lattice with a smaller hexagon, and showed that the elastic moduli of the hierarchical honeycombs with one level and two levels can be 2.0 and 3.5 times stiffer than their equal-mass regular hexagonal honeycomb, respectively. In a previous paper we [31] proposed multifunctional hierarchical honeycombs (MHH), which are formed by replacing the solid cell walls of an original regular hexagonal honeycomb (ORHH) with three different isotropic honeycomb sub-structures possessing hexagonal, triangular and Kagome lattices, respectively. Analytical results

* Corresponding author. Laboratory of Bio-Inspired & Graphene Nanomechanics, Department of Civil, Environmental and Mechanical Engineering, University of Trento, Via Mesiano 77, Trento I-38123, Italy. Tel.: +39 0461 282525; fax: +39 0461 282599.
E-mail address: nicola.pugno@unitn.it (N.M. Pugno).

0263-8223/$ - see front matter © 2013 The Authors. Published by Elsevier Ltd. All rights reserved.
http://dx.doi.org/10.1016/j.compstruct.2013.05.008

show that, compared with the ORHH, triangular and Kagome substructures could greatly increase the in plane Young's modulus of the MHH structure, up to 1 order or 3 orders of magnitude depending on the cell wall thickness-to-length ratio of the ORHH.

The concept of negative Poisson's ratio (NPR) can also be explored to improve the elastic moduli of regular hexagonal honeycombs. One of the two interesting NPR cellular solids are the anisotropic re-entrant honeycomb [32,33] and the isotropic (Poisson's ratio -1) chiral honeycomb [34]. The multifunctionality of these two kinds of honeycombs has been widely studied. Scarpa and Tomlinson [35] studied the vibration of a sandwich plate with re-entrant honeycomb cores and suggested that the dynamic performance of a sandwich structure could be significantly improved using the re-entrant cell cores. Ruzzene [36] analyzed the vibration and sound radiation of sandwich beams with re-entrant honeycomb truss cores and indicated that re-entrant configurations are generally more effective for vibration and sound transmission reduction applications. Innocenti and Scarpa [37] studied the thermal conductivity and heat transfer properties of the multi-re-entrant honeycomb structures and showed that this auxetic honeycomb configurations show higher out-of-plane conductivity, strong in-plane thermal anisotropy and the lowest peak temperatures during heat transfer between the bottom and top faces of honeycomb panels. Besides, numerical and experimental simulations showed that chiral honeycombs have attractive dynamic properties when used as the core of airfoils [38–40]. At the same time, Spadoni et al. [41] studied the phononic properties of the hexagonal chiral lattices and suggested this kind of cellular lattices as potential building blocks for the design of meta-materials of interest for acoustic wave-guiding applications.

In this paper, by substituting the solid cell wall of an ORHH with anisotropic re-entrant honeycombs or isotropic chiral honeycombs, two new kinds of MHH structures with NPR sub-structures are introduced. Based on the Euler beam theory, formulas for the in-plane Young's moduli of these two kinds of MHH structures are finally derived. The presented theory could be used in designing new tailorable hierarchical multifunctional honeycombs.

2. MHH with re-entrant honeycomb sub-structures

2.1. Basic theory

At first, we consider the MHH with anisotropic re-entrant honeycomb sub-structures (Fig. 1). Fig. 1a is an ORHH with cell-wall thickness and length denoted by t_0 and l_0, respectively; Fig. 1b is an equal-mass MHH with the cell-wall thickness and length denoted by t_1 and l_0, respectively. We can see that the cell-wall lengths of the ORHH and the MHH are identical. In particular, one of the MHH cell walls in Fig. 1b is shown in Fig. 1c. The cell-wall thickness, lengths parallel and inclined to the local direction 2 for re-entrant hexagonal cells are denoted by t_r, h_r and l_r respectively. The angle between the inclined cell wall and the local direction 1 is denoted by θ ($\theta < 0°$). The out-of-plane depth is a constant and identical for both structures.

For simplicity of the calculation we suppose that both the cell walls of the MHH structure and re-entrant honeycomb substructures are Euler beams. That is to say, under small deformations we only consider the bending of the cell walls of the MHH structure and the re-entrant honeycomb sub-structures, which requires that $t_1/l_0 < 0.25$, $t_r/h_r < 0.25$ and $t_r/l_r < 0.25$ [33]. Under the above assumptions we can approximately treat this MHH structure as isotropic, even though its cell walls are constituted by anisotropic re-entrant honeycomb substructures.

Here we define $h_r/l_r = \alpha$ and $t_r/l_r = \beta$. The geometry of Fig. 1c implies that:

$$l_0 = n(h_r + 2l_r\sin\theta) + (n+1)h_r = n(\alpha + 2\sin\theta)l_r + (n+1)\alpha l_r \quad (1)$$

where $n+1$ is the number of solid re-entrant hexagonal cell walls lying on the middle line of the MHH cell wall (e.g., in Fig. 1c, $n = 15$). Defining $\lambda = l_r/l_0$ as the hierarchical length ratio and rearranging Eq. (1) provides

$$\lambda = \frac{l_r}{l_0} = \frac{1}{n(\alpha + 2\sin\theta) + (n+1)\alpha} \quad (2)$$

Then, defining N as the number of re-entrant hexagonal cells away from the middle line of the MHH cell walls (e.g., in Fig. 1c, $N = 1$), from the geometric analysis we get the cell wall thickness of the MHH structure:

$$t_1 = 2l_r\cos\theta \times 2N + \frac{t_r}{2}\times 2 = (4N\cos\theta + \beta)l_r = (4N\cos\theta + \beta)\lambda l_0 \quad (3)$$

that is

$$\frac{t_1}{l_0} = \lambda(4N\cos\theta + \beta) \quad (4)$$

Then from the precondition $t_1/l_0 < 0.25$ we obtain $N_{\max}$, the upper bound of N:

$$N_{\max} = fl\left[\frac{1}{16\lambda\cos\theta}\right] \quad (5)$$

where 'fl[]' is the floor function, which denotes the largest integer not greater than the term in the bracket.

The mass equivalence between the cell wall of the ORHH and that of the MHH structure gives the following relationship (see Appendix A):

$$BD\beta^3 + (AD + BC)\beta^2 + AC\beta - E = 0 \quad (6)$$

in which $A = 2N(2n+1)(\alpha+2) + \alpha(n+1)$, $B = [2N(2n+1) - (n+1)]\left(\frac{1}{2}\tan\theta - \frac{1}{\cos\theta}\right)$, $C = 1 - \frac{2}{\sqrt{3}}N\lambda\cos\theta$, $D = -\frac{1}{2\sqrt{3}}\lambda$, $E = \frac{1}{\lambda^2}\left[\frac{t_0}{l_0} - \frac{1}{2\sqrt{3}}\left(\frac{t_0}{l_0}\right)^2\right]$. Through Newton's method we solve Eq. (6) and get the solutions for β. Then, through the precondition $\beta < 0.25$, we can obtain $N_{\min}$, the lower bound of N.

Defining E_O, E_M and E_{r2} as the in plane Young's moduli of the ORHH, MHH and the re-entrant honeycomb sub-structure in the local direction 2, we find [33]:

$$\frac{E_O}{E_s} = 2.3\left(\frac{t_0}{l_0}\right)^3 \quad (7)$$

$$\frac{E_M}{E_{r2}} = 2.3\left(\frac{t_1}{l_0}\right)^3 \quad (8)$$

$$\frac{E_{r2}}{E_s} = \left(\frac{t_r}{l_r}\right)^3\frac{h_r/l_r + \sin\theta}{\cos^3\theta} = \beta^3\frac{\alpha + \sin\theta}{\cos^3\theta} \quad (9)$$

There are some points needed to be noted here. In the first place, Eqs. (7)–(9) are only valid for infinite honeycombs, i.e., with large numbers of cells. Scarpa and collaborators studied the transverse shear stiffness of thickness gradient honeycombs [42] and the gradient cellular core for aeroengine fan blades based on auxetic configurations [43] and showed that low number of cells tend to decrease the stiffness compared to the infinite honeycomb case. Here for simplicity of the analytical analysis we use the ideal expressions Eqs. (7)–(9). In the second place, in Eq. (9) we neglect axial deformation of the ribs. This is true for internal cell angles roughly between $-60°$ and $-5°$, and 5–60°; smaller angles (in magnitude) would provide cellular configurations where rib stretching is dominant [44]. Finally, in Eq. (8) only E_{r2} is used to express the flexural stiffness E_M of the MHH. Because the re-entrant honeycomb sub-structure is treated as an Euler beam, for the MHH only the Young's modulus in the local direction 2, E_{r2}, is considered (for details, see [33]). Combining Eqs. (7)–(9) gives the relative Young's modulus E_M/E_O:

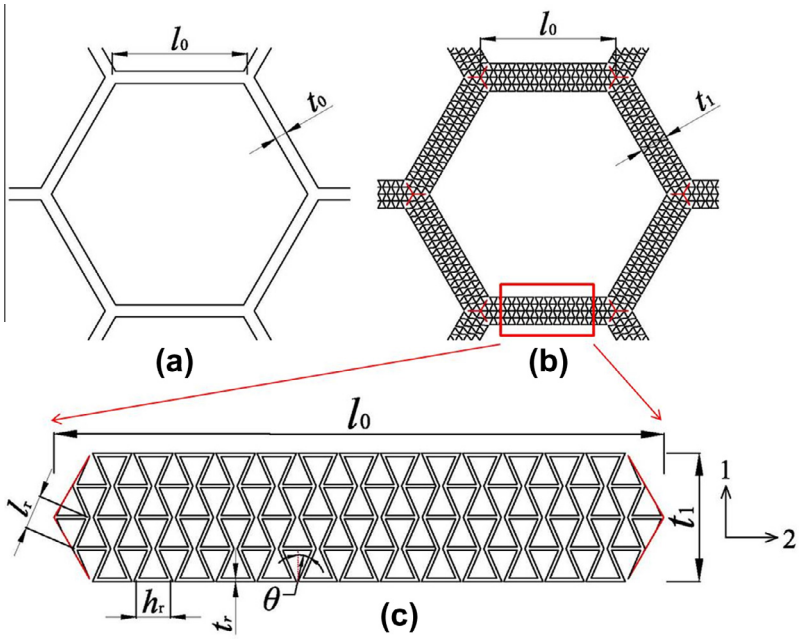

Fig. 1. (a) The original regular hexagonal honeycomb (ORHH); (b) the tailorable multifunctional hierarchical honeycomb (MHH) with re-entrant honeycomb sub-structures; and (c) amplification of a re-entrant hexagonal lattice cell wall in (b).

$$\frac{E_M}{E_O} = \frac{(t_1/l_0)^3 \beta^3 (\alpha + \sin\theta)}{(t_0/l_0)^3 \cos^3\theta} \tag{10}$$

2.2. Effects of α, N, t_0/l_0 and λ on the relative Young's moduli

To investigate the influence of N on the relative elastic moduli E_M/E_O, here we consider the following examples with parameters $n = 30$, $\theta = -5°$, $t_0/l_0 = 0.01$, 0.02, 0.03, 0.04, 0.045 and $\alpha = 1$, 1.5, 2 and 3. The results of E_M/E_O vs N for different t_0/l_0 are shown in Fig. 2. It is easy to see from Fig. 2 that in general E_M/E_O increases with the increases of N and α.

Comparing Eqs. 2(a)–(d) we can see that the parameter α has a vital influence on E_M/E_O, which can also be seen from Eq. (10). When $\alpha \leqslant 1.5$ the relative elastic moduli $E_M/E_O < 1$ (Fig. 2), which means that for $\alpha \leqslant 1.5$ the Young's modulus of the MHH structure with re-entrant honeycomb sub-structures is smaller than that of the ORHH. Note that when $t_0/l_0 > 0.045$ the assumptions in Section 2.1 are not satisfied. So here we only consider the case of $t_0/l_0 \leqslant 0.045$.

To see the effect of θ on E_M/E_O, we use the parameters $n = 30$, $\alpha = 3$, $t_0/l_0 = 0.01, 0.02, 0.03, 0.04$, $\theta = -60°$ to $-5°$. The results involving the maximum E_M/E_O and θ are given in Fig. 3. It is apparent that the maximum E_M/E_O decreases with the decrease of θ. At the same time, to see the effects of λ, i.e., n, on E_M/E_O, we study the parameters $\alpha = 4$, $\theta = -5°$, $t_0/l_0 = 0.01$, 0.03 and $n = 10$–50. The results are shown in Fig. 4a which shows that with the increase of n the maximum E_M/E_O increases in a sawtooth shape. The reason is due to the change of $N_{\max}$ with the increase of n. One example is given in Fig. 4b, in which E_M/E_O vs N for $n = 10$, 11, 12, 13 are plotted. It is easy to see that for $n = 10$ and 11, $N_{\max} = 5$; for $n = 12$ and 13, $N_{\max} = 6$; and connecting the maximum E_M/E_O corresponding to $n = 10$, 11, 12, 13, respectively, will produce the sawtooth shape shown in Fig. 4a.

3. MHH with isotropic chiral honeycomb sub-structures

3.1. Basic theory

In this section, we substitute the ORHH cell walls with equal-mass isotropic chiral honeycomb sub-structures, see Fig. 5. The cell wall thickness, the circular node radius, the distance between the centers of the adjacent circular cells and the length of the ligaments in the chiral honeycomb are denoted by t, r, R and l, respectively (Fig. 5d). Then the geometrical relation $r^2 + l^2/4 = R^2/4$ holds. We suppose $t/l < 0.25$ so that the Euler beam theory can be applied, i.e., only the bending of the ligaments is considered [33,34].

As defined in Section 3, here the hierarchical length ratio is expressed as

$$\lambda = \frac{R}{l_0} = \frac{1}{n} (n \geqslant 1) \tag{11}$$

where n is the number of the distance R lying on the middle line of the MHH cell walls. Supposing

$$\frac{R}{r} = k \tag{12}$$

and combining it with the relation $r^2 + l^2/4 = R^2/4$ gives:

$$\begin{cases} \frac{r}{l} = A = \frac{1}{\sqrt{k^2-4}} \\ \frac{l}{l_0} = B = \frac{\sqrt{k^2-4}}{nk} \\ \frac{R}{l} = C = \frac{k}{\sqrt{k^2-4}} \end{cases} \tag{13}$$

Defining N as the number of circular cells in the thickness direction of the cell wall of the MHH structure, similar to that done in Section 2, a geometrical analysis on Fig. 5c provides $N_{\max}$, the upper bound of N, and t_1, the thickness of the MHH cell walls:

$$N_{\max} = n \tag{14}$$

$$t_1 = \begin{cases} \sqrt{3}NR + 2t & 1 \leqslant N < N_{\max} \\ \sqrt{3} l_0 & N = N_{\max} \end{cases} \tag{15}$$

Then, rearranging Eq. (15) gives

$$\frac{t_1}{l_0} = \begin{cases} \frac{\sqrt{3}N}{n} + 2B\beta & 1 \leqslant N < N_{\max} \\ \sqrt{3} & N = N_{\max} \end{cases} \tag{16}$$

in which $\beta = t/l$ is the thickness-to-length ratio of the ligaments.

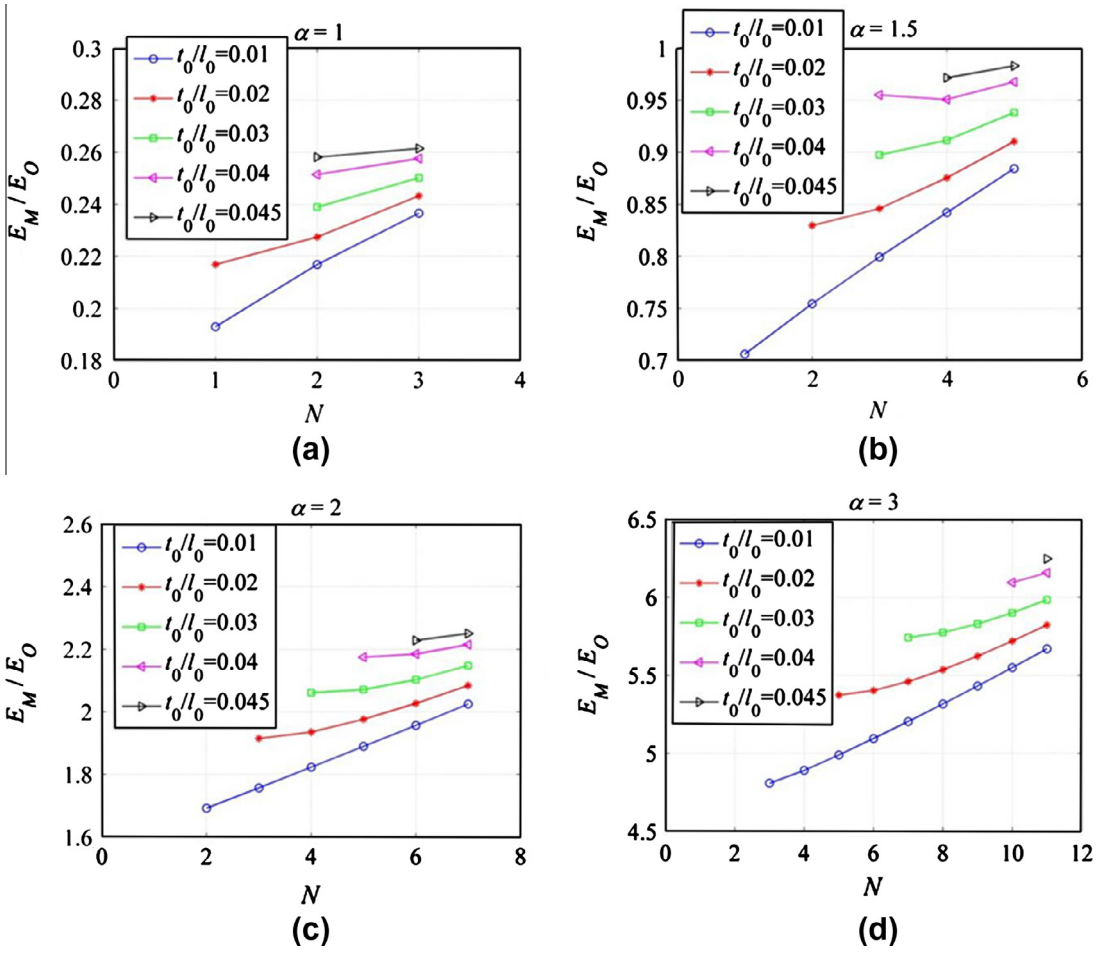

Fig. 2. The relative Young's modulus E_M/E_O vs N for different t_0/l_0 with (a) $\alpha = 1$; (b) $\alpha = 1.5$; (c) $\alpha = 2$; and (d) $\alpha = 3$.

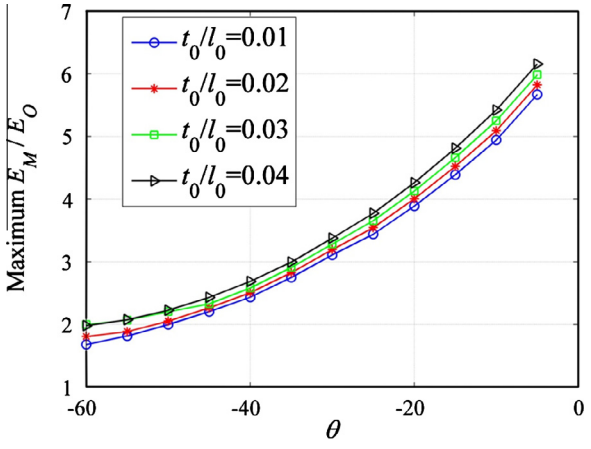

Fig. 3. The maximum E_M/E_O vs θ for different t_0/l_0.

If $N < N_{max}$, from Fig. 5c, according to the equal-mass principle, we can find

$$t_0 l_0 - \frac{1}{2\sqrt{3}} t_0^2 = MQ + 2(l_0 - NR)t = MQ + 2\left(\frac{1}{B} - NC\right)tl \tag{17}$$

where M is the total number of the circular cells in one cell wall of the MHH structure and Q is the in-plane areas of one circular cell and six half-length ligaments. In fact, one circular cell in the MHH cell wall corresponds to six half-length ligaments. M has the following relationship with n and N (see Appendix B):

$$M = N(2n - N)(1 \leqslant N \leqslant n) \tag{18}$$

and

$$\begin{aligned} Q &= \pi\left[\left(r+\frac{t}{2}\right)^2 + \left(r-\frac{t}{2}\right)^2\right] \\ &\quad + 6\left\{\frac{1}{2}tl - \left(\left(\frac{\pi}{2} - \tan^{-1}\sqrt{\frac{2r}{t}}\right)\left(r+\frac{t}{2}\right)^2 - \frac{1}{2}\left(r-\frac{t}{2}\right)\sqrt{2tr}\right)\right\} \\ &= 2\pi rt + 3tl - 6\left(\frac{\pi}{2} - \tan^{-1}\sqrt{\frac{2r}{t}}\right)\left(r+\frac{t}{2}\right)^2 + 3\left(r-\frac{t}{2}\right)\sqrt{2tr} \end{aligned} \tag{19}$$

Then, rearranging Eq. (17) gives

$$\begin{aligned} &\left(2\pi A + 3 + \frac{2}{BM} - \frac{2NC}{M}\right)\beta - 6\left(\frac{\pi}{2} - \tan^{-1}\sqrt{\frac{2A}{\beta}}\right)\left(A + \frac{1}{2}\beta\right)^2 \\ &+ 3\left(A - \frac{1}{2}\beta\right)\sqrt{2A\beta} \\ &= \frac{1}{B^2 M}\left[\frac{t_0}{l_0} - \frac{1}{2\sqrt{3}}\left(\frac{t_0}{l_0}\right)^2\right] \end{aligned} \tag{20}$$

When $N = N_{max}$, it gives

$$t_0 l_0 - \frac{1}{2\sqrt{3}} t_0^2 = MQ + 2(l_0 - NR)t = MQ \tag{21}$$

and rearranging Eq. (21) we obtain

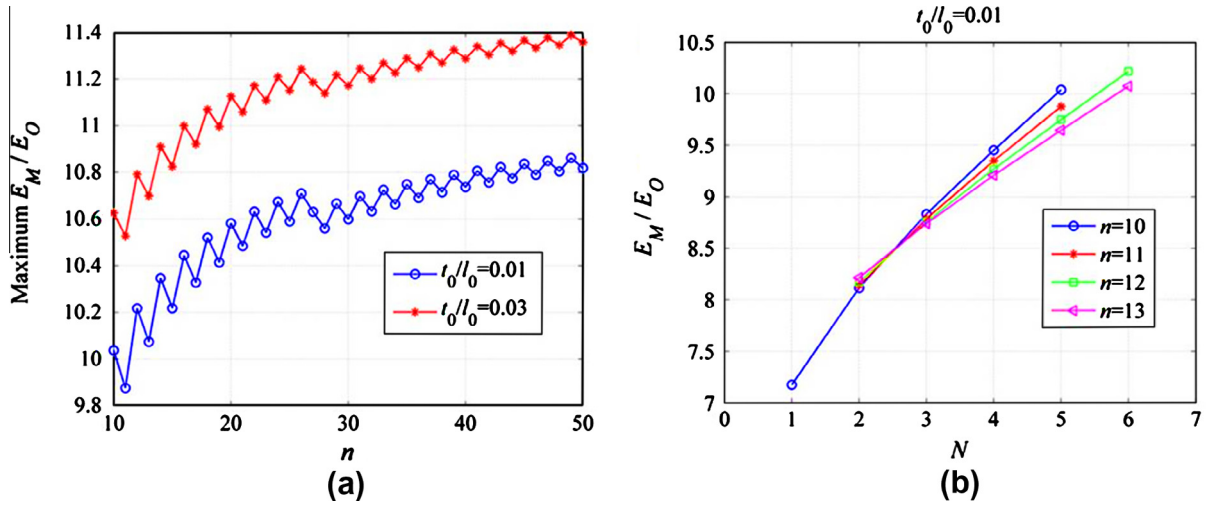

Fig. 4. (a) The maximum E_M/E_O vs n for different t_0/l_0; and (b) E_M/E_O vs N for different n with $t_0/l_0 = 0.01$.

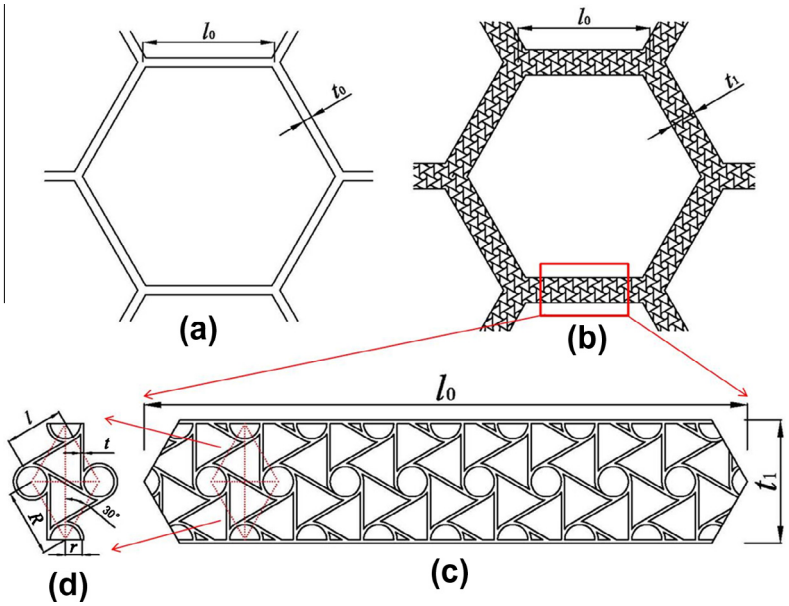

Fig. 5. Schematics of (a) the ORHH; (b) the tailorable MHH with chiral honeycomb sub-structures; (c) amplification of a chiral lattice cell wall in (b); and (d) geometrical parameters of the chiral honeycomb cell in (c).

$$(2\pi A+3)\beta-6\left(\frac{\pi}{2}-\tan^{-1}\sqrt{\frac{2A}{\beta}}\right)\left(A+\frac{1}{2}\beta\right)^2+3\left(A-\frac{1}{2}\beta\right)\sqrt{2A\beta}=\frac{1}{B^2M}\left[\frac{t_0}{l_0}-\frac{1}{2\sqrt{3}}\left(\frac{t_0}{l_0}\right)^2\right] \tag{22}$$

Through Newton's method we can solve Eqs. (20) and (22) and get the solutions for β. Then from the precondition $\beta < 0.25$ we can obtain $N_{\min}$, the lower bound of N.

In a previous paper we derived analytical formulas for the Young's modulus of the regular hexagonal honeycomb at all densities [31]. Defining E_O, E_M and E_C as the in plane Young's moduli of the ORHH, MHH and the chiral honeycomb sub-structures, using our previous results and referring to the results of Prall and Lakes [34], we find:

$$\frac{E_O}{E_s}=A_O=\begin{cases}\frac{3}{2}\phi_O^3 & \phi_O\leqslant 0.5\\ \frac{\phi_O(2\zeta_O-1)(\zeta_O+\eta_O-1)}{\{3-2\phi_O-2(2-\phi_O)(1-\zeta_O)+(2-\zeta_O-\eta_O)[2\phi_O(1-\zeta_O)-1]\}} & \phi_O>0.5\end{cases} \tag{23}$$

$$\frac{E_M}{E_C}=A_M=\begin{cases}\frac{3}{2}\phi_M^3 & \phi_M\leqslant 0.5\\ \frac{\phi_M(2\zeta_M-1)(\zeta_M+\eta_M-1)}{\{3-2\phi_M-2(2-\phi_M)(1-\zeta_M)+(2-\zeta_M-\eta_M)[2\phi_M(1-\zeta_M)-1]\}} & \phi_M>0.5\end{cases} \tag{24}$$

$$\frac{E_C}{E_s}=A_c=\sqrt{3}\left(\frac{t}{l}\right)^3\left(\frac{l}{r}\right)^2=\sqrt{3}\beta^3\frac{1}{A^2} \tag{25}$$

in which

$$\phi_O=\frac{2}{\sqrt{3}}\frac{t_0}{l_0}-\frac{1}{3}\left(\frac{t_0}{l_0}\right)^2\left(\frac{t_0}{l_0}\leqslant\sqrt{3}\right), \tag{26}$$

$$\phi_M=\frac{2}{\sqrt{3}}\frac{t_1}{l_0}-\frac{1}{3}\left(\frac{t_1}{l_0}\right)^2\left(\frac{t_1}{l_0}\leqslant\sqrt{3}\right), \tag{27}$$

ζ_O and η_O, ζ_M and η_M, interpolated from Fig. 6, are the three-point parameters corresponding to ϕ_O and ϕ_M respectively; E_s is the Young's modulus of the solid of which the ORHH is made. Combining Eqs. (22)–(25) gives the relative Young's modulus E_M/E_O:

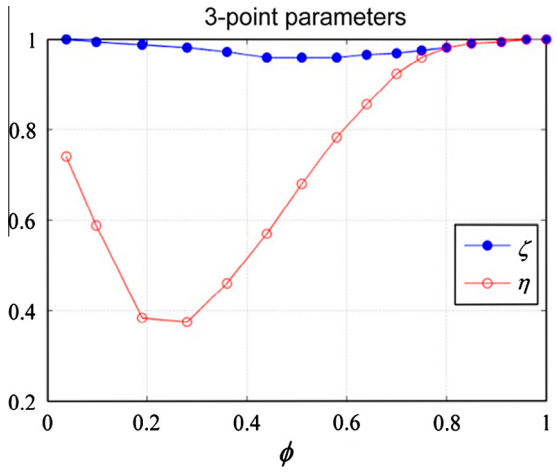

Fig. 6. Three-point parameters ζ and η for the regular hexagonal honeycomb vs the relative density ϕ [31].

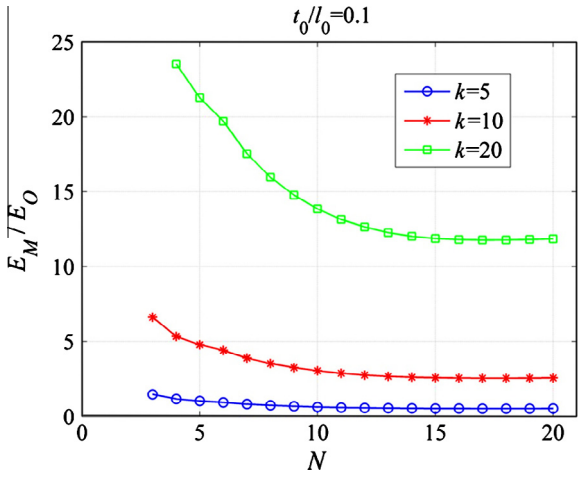

Fig. 9. E_M/E_O vs N for different k.

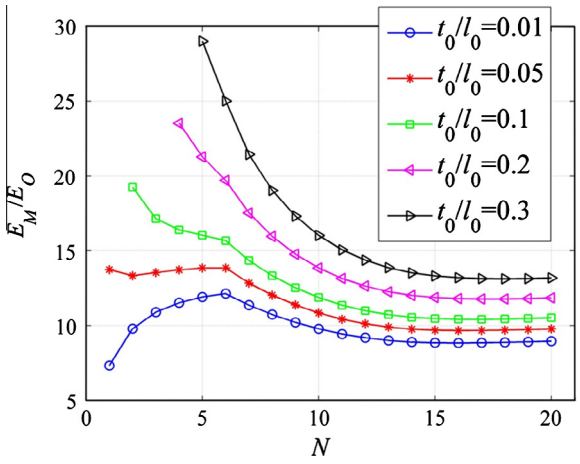

Fig. 7. The relative Young's modulus E_M/E_O vs N for different t_0/l_0.

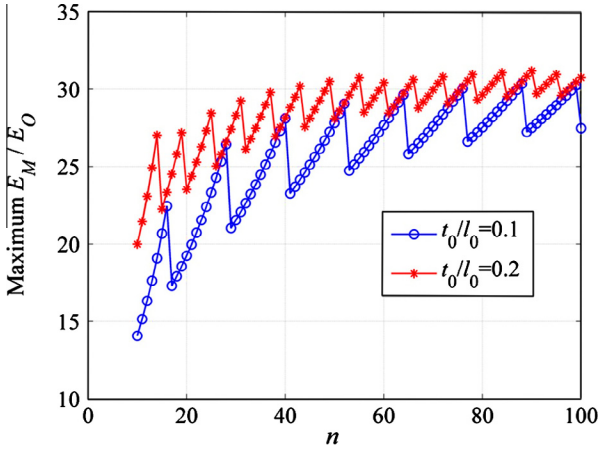

Fig. 10. The maximum E_M/E_O vs n for different t_0/l_0.

$$\frac{E_M}{E_O} = \frac{A_M A_c}{A_O} \tag{28}$$

3.2. Effects of N, t_0/l_0, k and λ on the relative Young's moduli

Similar to Section 2, in order to investigate the effect of N on the relative Young's moduli E_M/E_O, we consider here the following parameters $n = 20$, $k = 20$, $t_0/l_0 = 0.01$, 0.05, 0.1, 0.2 and 0.3. The results of E_M/E_O vs N for the above mentioned t_0/l_0 values are shown in Fig. 7. From Fig. 7 we can see that different t_0/l_0 ratios correspond to different ranges of N. For $t_0/l_0 = 0.01$ and 0.05 peak values of E_M/E_O exist at $N = 6$, for $t_0/l_0 = 0.1$, 0.2 and 0.3 in general E_M/E_O decreases with the increase of N. Note that when $t_0/l_0 > 0.75$, $N_{\min} \leqslant N \leqslant N_{\max}$ cannot be satisfied for any value of N. So the theory

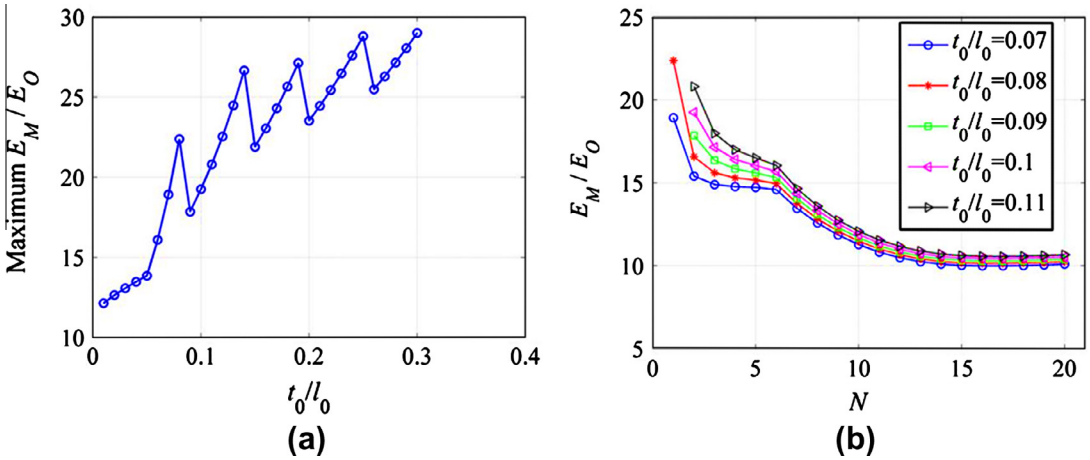

Fig. 8. (a) The maximum E_M/E_O vs t_0/l_0; and (b) E_M/E_O vs N for different t_0/l_0.

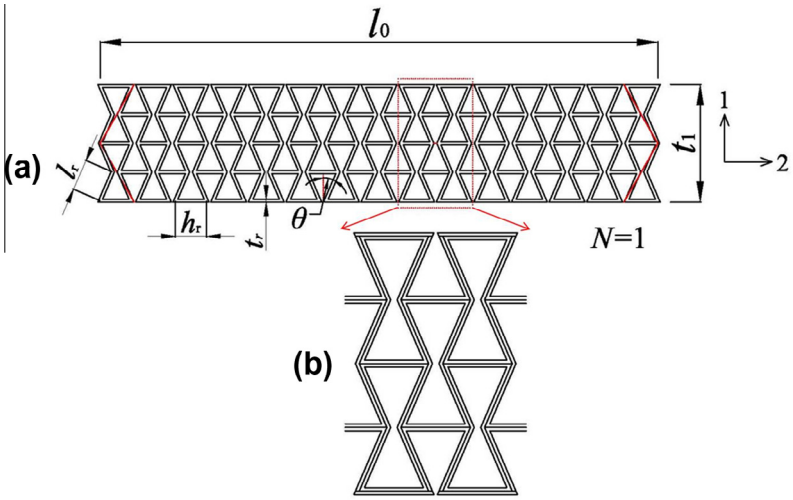

Fig. A.1. (a) Schematics for the representative cell walls of the MHH with re-entrant honeycomb sub-structures ($N = 1$) shown in Fig. 1b; and (b) details of the re-entrant cells in (a).

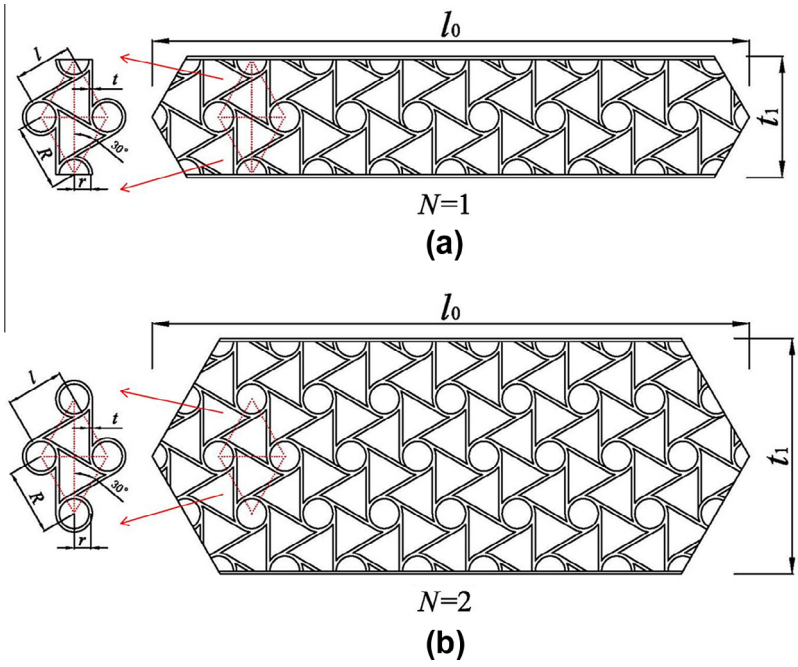

Fig. B.1. Schematics for the representative cell walls of the MHH with chiral honeycomb sub-structures: (a) $N = 1$; and (b) $N = 2$.

here is only suitable for the ORHH with the thickness-to-length ratio t_0/l_0 less than 0.75.

To see the effect of t_0/l_0 on E_M/E_O, we use the parameters $n = 20$, $k = 20$ and $t_0/l_0 = 0.01$–0.3. The results involving the maximum E_M/E_O and t_0/l_0 are shown in Fig. 8a, which indicates that with the increase of n the maximum E_M/E_O increases in a sawtooth shape. The reason of this kind of shape is due to the change of the range of N with the increase of t_0/l_0. One example is given in Fig. 8b, in which E_M/E_O vs N for $t_0/l_0 = 0.07, 0.08, 0.09, 0.10, 0.11$ are plotted. It is easy to see that connecting the maximum E_M/E_O corresponding to $t_0/l_0 = 0.07, 0.08, 0.09, 0.10, 0.11$, respectively, will produce the sawtooth shape shown in Fig. 8a.

To see the effect of k on E_M/E_O, we consider the parameters $n = 20$, $t_0/l_0 = 0.1$ and $k = 5$, 10, 20. The results are shown in Fig. 9. Apparently E_M/E_O increases with the increase of k. Finally, to see the effects of λ, i.e., n, on E_M/E_O, we investigate the parameters $k = 20$, $t_0/l_0 = 0.1$, 0.2 and $n = 10$–100. The related results are shown in Fig. 10. We can see that the maximum E_M/E_O also increases in a sawtooth shape with the increase of n. As in Fig. 8, the reason is also due to the change of the range of N with the increase of n.

4. Conclusions

In this paper, by substituting the solid cell walls of the original regular hexagonal honeycomb (ORHH) with two equal mass NPR honeycombs, the re-entrant honeycomb and the isotropic chiral honeycomb, two new kinds of multifunctional hierarchical honeycombs are proposed. Based on the Euler beam theory, the analytical formulas for the Young's moduli of these two new MHH

structures are derived. Analytical analysis indicates that both the re-entrant honeycomb sub-structures and the chiral honeycomb substructures can greatly increase the in-plane stiffness of the MHH by appropriately designing its geometry. This paper shows the possibility to design new hexagonal honeycombs for multi-functional applications, which combine the advantages of hierarchical and NPR materials.

Acknowledgements

The research related to these results has received funding from the European Research Council under the European Union's Seventh Framework Programme (FP7/2007-2013)/ERC Grant Agreement No. [279985] (ERC Starting Grant, on 2011 BIHSNAM "Bio-inspired hierarchical super nanomaterials" PI NMP). Y. Sun appreciates the China Scholarship Council (CSC) for the financial supports and Q. Chen for the insightful discussions.

Appendix A. MHH cell wall with re-entrant honeycomb sub-structures

In this appendix the mass equivalence between the cell walls of the ORHH and the MHH with re-entrant honeycomb sub-structures is derived. As shown in Fig. A.1a, the cell walls of the MHH with re-entrant honeycomb sub-structures are fabricated by cutting the rectangular re-entrant honeycomb beams at the four red lines. The angles between the four red lines and the local direction 2 are all 60°. So the cell wall mass of the ORHH is equal to the mass encased by the four red lines (Fig. A.1a).

Supposing the density of the solid of which the ORHH is made and the out-of-plane depth of the MHH structure are both 1, from geometrical analysis it is easy to obtain the following parameters. The mass/area of one half-thickness re-entrant honeycomb cell is

$$\begin{aligned} A' &= 2t_r l_r + \left[h_r + \left(\frac{1}{2}\tan\theta - \frac{1}{\cos\theta}\right)t_r\right]t_r \\ &= (h_r + 2l_r)t_r + \left(\frac{1}{2}\tan\theta - \frac{1}{\cos\theta}\right)t_r^2 \\ &= (\alpha+2)t_r l_r + \left(\frac{1}{2}\tan\theta - \frac{1}{\cos\theta}\right)t_r^2 \end{aligned} \tag{A.1}$$

The number of the half-thickness re-entrant honeycomb cells in the uncut beam is

$$B' = 2N(n+n+1) = 2N(2n+1) \tag{A.2}$$

The number of the half-thickness cell walls in the two outward sides is

$$C' = 2(n+1) \tag{A.3}$$

The mass of one half-thickness cell wall in the two outward sides is:

$$\begin{aligned} D' &= \left(h_r + 2\frac{t_r/2}{\cos\theta} + h_r + 2\frac{t_r/2}{\cos\theta} - 2\frac{t_r}{2}\tan\theta\right)\frac{t_r}{2}\times\frac{1}{2} \\ &= \frac{1}{2}h_r t_r + \frac{1}{4}t_r^2\left(\frac{2}{\cos\theta} - \tan\theta\right) \\ &= \frac{1}{2}\alpha l_r t_r + \frac{1}{4}t_r^2\left(\frac{2}{\cos\theta} - \tan\theta\right) \end{aligned} \tag{A.4}$$

The ratio of the area encased by the four red lines is

$$\begin{aligned} E' &= 1 - \frac{\frac{1}{2}\times\frac{t_1}{2}\times\frac{t_1}{2}\times\frac{1}{\sqrt{3}}\times 4}{t_1 l_0} = 1 - \frac{1}{2\sqrt{3}}\frac{t_1}{l_0} \\ &= 1 - \frac{1}{2\sqrt{3}}\lambda(4N\cos\theta + \beta) \end{aligned} \tag{A.5}$$

Then the mass equivalence between the cell walls of the ORHH and the MHH with re-entrant honeycomb sub-structures gives [31]

$$(A'B' + C'D')E' = t_0 l_0 - \frac{1}{2\sqrt{3}}t_0^2 \tag{A.6}$$

Rearranging Eq. (A.6) gives

$$BD\beta^3 + (AD + BC)\beta^2 + AC\beta - E = 0 \tag{A.7}$$

in which $A = 2N(2n+1)(\alpha+2) + \alpha(n+1)$, $B = [2N(2n+1) - (n+1)]\left(\frac{1}{2}\tan\theta - \frac{1}{\cos\theta}\right)$, $C = 1 - \frac{2}{\sqrt{3}}N\lambda\cos\theta$, $D = -\frac{1}{2\sqrt{3}}\lambda$, $E = \frac{1}{\lambda^2}\left[\frac{t_0}{l_0} - \frac{1}{2\sqrt{3}}\left(\frac{t_0}{l_0}\right)^2\right]$.

Appendix B. MHH cell wall with chiral honeycomb sub-structures

Fig. B.1 schematically shows the cell walls of the MHH with chiral honeycomb sub-structures (Fig. 5b). The hierarchical length ratio is $\lambda = 1/n$. M is the number of the circular cells in one cell wall of the MHH structure, N is the number of circular cells in the thickness direction of the cell wall. It is easy to get the following relation between M, N and n:

$$\begin{aligned} N = 1 : M &= (n-1) + (n-2) + 2 = 2n - (1+2) + 2\times 1 \\ N = 2 : M &= (n-1) + 2(n-2) + (n-3) + 2 + \frac{1}{2}\times 4 \\ &= 4n - (1+2) - (2+3) + 2\times 2 \\ N = 3 : M &= (n-1) + 2(n-2) + 2(n-3) + (n-4) + 2 + \frac{1}{2}\times 8 \\ &= 6n - (1+2+3) - (2+3+4) + 2\times 3 \end{aligned} \tag{B.1}$$

Then, recursively, we find

$$M = N(2n-N)(1 \leqslant N \leqslant n) \tag{B.2}$$

References

[1] Wilson S. A new face of aerospace honeycomb. Mater Des 1990;11(6):323–6.
[2] Bitzer T. Honeycomb marine applications. J Reinf Plast Compos 1994;13(4):355–60.
[3] Thompson RW, Matthews FL. Load attachments for honeycomb panels in racing cars. Mater Des 1995;16(3):131–50.
[4] Price T, Timbrook RL. Structural honeycomb panel building system, Patent number US6, 253, 530 B1. July 3, 2001.
[5] Lu TJ. Heat transfer efficiency of metal honeycombs. Int J Heat Mass Transfer 1999;42(11):2031–40.
[6] Gu S, Lu TJ, Evans AG. On the design of two-dimensional cellular metals for combined heat dissipation and structural load capacity. Int J Heat Mass Transfer 2001;44(11):2163–75.
[7] Hyun S, Torquato S. Optimal and manufacturable two-dimensional, Kagome-like cellular solids. J Mater Res 2002;17(1):137–44.
[8] Wen T, Tian J, Lu TJ, Queheillalt DT, Wadley HNG. Forced convection in metallic honeycomb structures. Int J Heat Mass Transfer 2006;49:3313–24.
[9] Wang Bo, Wang Bin, Cheng G. Multifunctional design of sandwich panels with Kagome-like cores. Acta Materiae Compos Sinica 2007;24(3):109–15.
[10] Lakes R. Materials with structural hierarchy. Nature 1993;361:511–5.
[11] Pugno N. Mimicking nacre with super-nanotubes for producing optimized super-composites. Nanotechnology 2006;17(21):5480–4.
[12] Gao H. Application of fracture mechanics concepts to hierarchical biomechanics of bone and bone-like materials. Int J Fract 2006;138:101–37.
[13] Pugno N, Carpinteri A. Design of micro-nanoscale bio-inspired hierarchical materials. Philos Mag Lett 2008;88(6):397–405.
[14] Carpinteri A, Pugno N. Mechanics of hierarchical materials. Int J Fract 2008;150:221–6.
[15] Zhao Q, Kreplak L, Buehler MJ. Hierarchical structure controls nanomechanical properties of vimentin intermediate filaments. PLoS ONE 2009;4(10):e7294.
[16] Fratzl P, Weinkamer R. Nature's hierarchical materials. Progr Mater Sci 2007;52:1263–334.
[17] Chen Q, Pugno N. Modeling the elastic anisotropy of woven hierarchical tissues. Compos Part B: Eng 2011;42(7):2030–7.
[18] Chen Q, Pugno N. Mechanics of hierarchical 3-D nanofoams. Europhys Lett 2012;97:26002.
[19] Burgueno R, Quagliata MJ, Mohanty AK, Mehtad G, Drzale LT, Misraf M. Hierarchical cellular designs for load-bearing biocomposite beams and plates. Mater Sci Eng A 2005;390:178–87.
[20] Fan H, Jin F, Fang D. Mechanical properties of hierarchical cellular materials. Part I: Analysis. Compos Sci Technol 2008;68:3380–7.

[21] Garcia AP, Pugno N, Buehler MJ. Superductile, wavy silica nanostructures inspired by diatom algae. Adv Eng Mater 2011;13(10):B405–14.
[22] Zhao L, Zheng Q, Fan H, Jin F. Hierarchical composite honeycombs. Mater Des 2012;40:124–9.
[23] Pugno N, Chen Q. In plane elastic properties of hierarchical cellular solids. Eng Procedia, Phys Eng 2011;10:3026–31.
[24] Chen Q, Pugno N. In-plane elastic buckling of hierarchical honeycomb materials. Eur J Mech A/Solids 2012;34:120–9.
[25] Chen Q, Pugno N. Competition between in-plane buckling and bending collapses in nano-honeycombs. Europhys Lett 2012;98:16005.
[26] Chen Q, Pugno N. Bio-mimetic mechanisms of natural hierarchical materials: a review. J Mech Behavior Biomed Mater 2013;19:3–33.
[27] Sun Y, Pugno N. Hierarchical fibers with a negative Poisson's ratio for tougher composites. Materials 2013;6(2):699–712.
[28] Taylor CM, Smith CW, Miller W, Evans KE. The Effects of hierarchy on the in-plane elastic properties of honeycombs. Int J Solids Struct 2011;48:1330–9.
[29] Taylor CM, Smith CW, Miller W, Evans KE. Functional grading in hierarchical honeycombs: density specific elastic performance. Compos Struct 2012;94:2296–305.
[30] Ajdari A, Jahromi BH, Papadopoulos J, Nayeb-Hashemi H, Vaziri A. Hierarchical honeycombs with tailorable properties. Int J Solids Struct 2012;49:1413–19.
[31] Sun Y, Chen Q, Pugno N. Elastic and transport properties of the tailorable multifunctional hierarchical honeycombs, submitted for publication.
[32] Masters IG, Evans KE. Models for the elastic deformation of honeycombs. Compos Struct 1996;35(4):403–22.
[33] Gibson LJ, Ashby MF. Cellular solids, structures and properties. 2nd ed. Cambridge: Cambridge University Press; 1997.
[34] Prall D, Lakes RS. Properties of a chiral honeycomb with a Poisson's ratio −1. Int J Mech Sci 1996;39(3):305–14.
[35] Scarpa F, Tomlinson G. Theoretical characteristics of the vibration of sandwich plates with in-plane negative Poisson's ratio values. J Sound Vib 2000;230(1):45–67.
[36] Ruzzene M. Vibration and sound radiation of sandwich beams with honeycomb truss core. J Sound Vib 2004;277:741–63.
[37] Innocenti P, Scarpa F. Thermal conductivity properties and heat transfer analysis of multi-re-entrant auxetic honeycomb structures. J Compos Mater 2009;43(21):2419–39.
[38] Spadoni A, Ruzzene M, Scarpa F. Dynamic response of chiral truss-core assemblies. J Intell Mater Syst Struct 2006;17(11):941–52.
[39] Spadoni A, Ruzzene M. Numerical and experimental analysis of the static compliance of chiral truss-core airfoils. J Mech Mater Struct 2007;2(5):965–81.
[40] Bettini P, Airoldi A, Sala G, Di Landro L, Ruzzene M, Spadoni A. Composite chiral structures for morphing airfoils: numerical analyses and development of a manufacturing process. Composites: Part B 2009. doi:10.1016/j.compositesb.2009.10.005.
[41] Spadoni A, Ruzzene M, Gonella S, Scarpa F. Phononic characteristics of hexagonal chiral lattices. Wave Motion 2009;46(7):435–50.
[42] Lira C, Scarpa F. Transverse shear stiffness of thickness gradient honeycombs. Compos Sci Technol 2010;70(6):930–6.
[43] Lira C, Scarpa F, Rajasekaran R. A gradient cellular core for aeroengine fan blades based on auxetic configurations. J Intell Mater Syst Struct 2011;22:907–17.
[44] Scarpa F, Panayiotou P, Tomlinson G. Numerical and experimental uniaxial loading on in-plane auxetic honeycombs. J Strain Anal Eng Des 2000;35(5):383–8.